

AN INDIUM GALLIUM ARSENIDE VISIBLE/SWIR FOCAL PLANE ARRAY FOR LOW LIGHT LEVEL IMAGING

August 1999

Marshall J. Cohen, Martin H. Ettenberg, Michael J. Lange, and Gregory H. Olsen
Sensors Unlimited, Inc.
3490 US Route 1
Princeton, NJ 08540
(609) 520-0610 (tel)
(609) 520-0638 (fax)
mjcsensors@aol.com

ABSTRACT

PIN photodiodes fabricated from indium gallium arsenide lattice-matched to indium phosphide substrates ($\text{In}_{.53}\text{Ga}_{.47}\text{As}/\text{InP}$) exhibit low reverse saturation current densities ($J_D < 10^{-8} \text{ A/cm}^2$), and high shunt resistance-area products ($R_o A > 10^6 \Omega\text{-cm}^2$) at $T=290\text{K}$. Backside-illuminated, hybrid-integrated InGaAs FPAs are sensitive from $0.9 \mu\text{m}$ to $1.7 \mu\text{m}$. 290K detectivities, D^* , greater than $10^{14} \text{ cm}\sqrt{\text{Hz/W}}$ are demonstrated. **This represents the highest room temperature detectivity of any infrared material.**

The long wavelength cutoff ($1.7 \mu\text{m}$) makes $\text{In}_{.53}\text{Ga}_{.47}\text{As}$ an idea match to the available airglow that has major peaks at $1.3 \mu\text{m}$ and $1.6 \mu\text{m}$. The short wavelength "cut-on" at $0.9 \mu\text{m}$ is due to absorption in the InP substrate. We will report on new InGaAs FPA epitaxial structures and processing techniques. These have resulted in improved performance in the form of a 10 x increase in detectivity and visible response via removal of the InP substrate. The resulting device features visible **and** SWIR response with greater than 15% quantum efficiency at $0.5 \mu\text{m}$ while maintaining the long wavelength cutoff. Imaging has been demonstrated under overcast starlight/urban glow conditions with cooling provided by a single stage thermoelectric cooler. Details on the material structure and device fabrication, quantitative characterization of spectral response and detectivity, as well as examples of night vision imagery are presented.

Form SF298 Citation Data

Report Date <i>("DD MON YYYY")</i> 00081999	Report Type N/A	Dates Covered (from... to) <i>("DD MON YYYY")</i>
Title and Subtitle An Indium Gallium Arsenide Visible/SWIR Focal Plane Array for Low Light Level Imaging		Contract or Grant Number
Authors Cohen, Marshall J.; Ettenberg, Martin H.; Lange, Michael J.; Olsen, Gregory H.		Program Element Number
Performing Organization Name(s) and Address(es) Sensors Unlimited, Inc. 3490 US Route 1 Princeton, NJ 08540		Project Number
Sponsoring/Monitoring Agency Name(s) and Address(es)		Task Number
Distribution/Availability Statement Approved for public release, distribution unlimited		Work Unit Number
Supplementary Notes		Performing Organization Number(s)
Abstract		Monitoring Agency Acronym
Subject Terms		Monitoring Agency Report Number(s)
Document Classification unclassified	Classification of SF298 unclassified	
Classification of Abstract unclassified	Limitation of Abstract unlimited	
Number of Pages 13		

1.0 INTRODUCTION

Military uses for the long-wave infrared (LWIR) and mid-wave infrared (MWIR) for thermal imaging have been explored in detail for many years. The short-wave infrared band (SWIR) has been neglected due to a lack of high performance imaging devices. Cameras incorporating InGaAs focal plane arrays have already been used to study potential military applications.^{1,2} There are many military imaging applications becoming apparent in the SWIR band that are not possible in the MWIR or LWIR. Some of the important applications are: low-light-level imaging utilizing the natural glow of the night sky, visualization of camouflaged objects and personnel, and imaging eye-safe lasers used for targeting, range-finding, illumination, and communications.

InGaAs FPAs operate at room temperature with high performance; for most applications active cooling is not required. Cameras incorporating InGaAs FPAs are thus excellent candidates for miniaturization and deployment in man-portable applications such as weapon sites, helmet-mounted imagers, and unmanned aerial vehicles (UAVs).

Potential materials for SWIR imaging include mercury cadmium telluride (MCT), indium antimonide (InSb), platinum silicide (PtSi), and InGaAs. Short wave MCT is highly mismatched to its substrate and suffers from high dark current.³ InSb and PtSi both require cryogenic cooling.

InGaAs has been extensively used in the fiber optic communication industry for over 15 years.^{4,5,6} This large commercial application has driven lattice-matched $\text{In}_{.53}\text{Ga}_{.47}\text{As}$ photodiode technology to the point where high-volume fabrication on 2-inch substrates is routine. A program is in place at Sensors Unlimited to develop the capability of producing InGaAs photodiode arrays on 100 mm InP substrates.⁷

Indium gallium arsenide ($\text{In}_x\text{Ga}_{1-x}\text{As}$) is an alloy of indium arsenide (InAs) and gallium arsenide (GaAs). The lattice-constants versus alloy composition of the InGaAsP quaternary system are shown in Figure 1. The alloy $\text{In}_{.53}\text{Ga}_{.47}\text{As}$ has the same lattice constant as indium phosphide.⁸ This lattice matching leads to high quality single-crystal epitaxial growth with low dark-current densities on the order of $3 \times 10^{-8} \text{ A/cm}^2$ and shunt resistance-area products (R_0A) in excess of $2 \times 10^6 \Omega\text{-cm}^2$.^{3,9} This has led to a detectivity, D^* , in excess of $10^{13} \text{ cm}\sqrt{\text{Hz/W}}$ at 290K increasing to $10^{14} \text{ cm}\sqrt{\text{Hz/W}}$ at 250K.

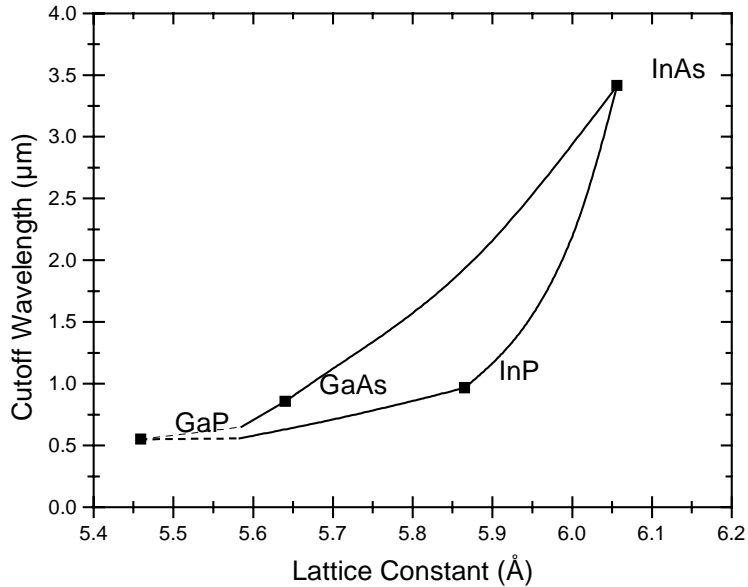


Figure 1. Cutoff wavelength versus lattice constant for the InGaAsP quaternary alloy system.

Lattice-matched $\text{In}_{.53}\text{Ga}_{.47}\text{As}$ is responsive from $0.9 \mu\text{m}$ to $1.7 \mu\text{m}$ in the SWIR band (Figure 2). The long wavelength cutoff corresponds to the energy bandgap of the active layer. The short wavelength “cut-on” is due to absorption in the InP substrate; the InGaAs, itself, is responsive throughout the visible wavelength band to $\lambda \sim 0.4 \mu\text{m}$. Figure 2 also shows the radiance of the night sky in the absence of moonlight or starlight.¹⁰ These curves indicate that InGaAs FPAs are excellent candidates for night vision imaging.

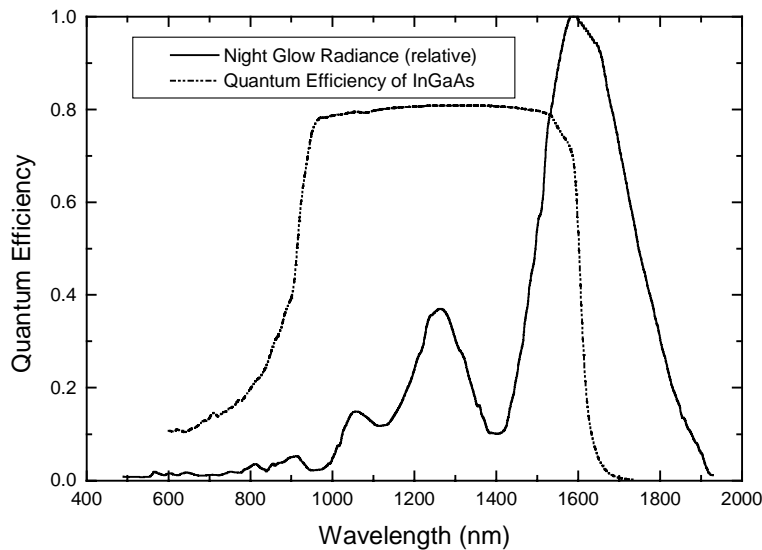


Figure 2. Quantum Efficiency of InGaAs versus radiance of the night sky in the absence of moonlight or starlight.

In this paper, we present results from two activities. We have modified the InGaAs epitaxial and device structures realizing a 10x increase in the detectivity and we have developed a novel epitaxial structure and processing technology that allows us to remove the InP substrate and buffer layer after the FPA has been hybridized. The result is a photodiode array structure that is less than 5 μm thick that responds from below 0.5 μm in the visible to 1.7 μm in the SWIR and capable of imaging under starlight conditions.

Increased Detectivity via Junction Miniaturization

The detectivity of an FPA is proportional to its signal-to-noise ratio, i.e. the photoresponse divided by the dark noise. For devices operated under bias, the dark noise is proportional to the square root of the dark current density. For devices operated at zero bias, the dark noise is inversely proportional to the square root of the shunt resistance-area product (RoA). In p-i-n photodiodes, the dark current decreases and the shunt resistance increases with decreasing junction area.

As the junction area decreases, the fill factor (junction area \div pixel area) decreases **linearly** while the dark noise decreases as the **square root** of the junction area. In order to realize an **increase** in detectivity, it is necessary that the pixel photoresponse be maintained as the junction area decreases.

To test the effect on D^* of decreasing the junction fill factor, we fabricated a 128x128 element photodiode array with 60 μm pixels. The photodiode array was divided into 8 sections, each containing 16 rows of pixels (Figure 3). The junction fill factors ranged from 44% (40 μm square junctions in the 60 μm square pixel) to 2% (10 μm diameter circular junctions in the 60 μm square pixels). The photodiode array was integrated with a Rockwell TCM-1700³ gate-modulated readout integrated circuit.

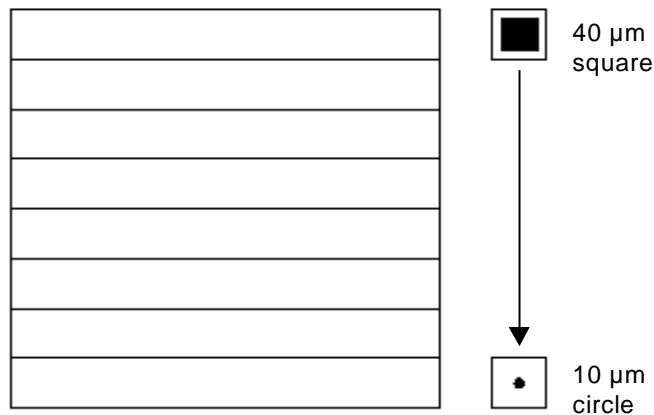


Figure 3. Test 128x128 element InGaAs FPA containing 8 sections of 16 rows. The junction fill factor ranged from 44% (40 μm square in 60 μm pixel) to 2% (10 μm diameter circle in 60 μm pixel).

Using an integrating sphere and a 1.55 μm laser diode, both dark and bright fields were acquired. Figure 4 shows the average dark and photo-signals for each section of pixels as a function of junction fill factor. The expected result was that the dark signal decreased with decreasing junction fill factor. The unexpected result was that not only did the photo-signal not decrease, it actually **increased** with decreasing fill factor.

These results derive from the current mirror architecture of the TCM-1700. In the gate-modulated detector interface,¹¹ the current gain increases with increasing photodiode impedance. The data in Figure 4 reflect the fact that both the dark current and the photocurrent are amplified prior to integration. As will be seen later, this gain is largely “noiseless.” While the currents are amplified, the output noise remains approximately constant so that the input-referenced signal-to-noise increases.

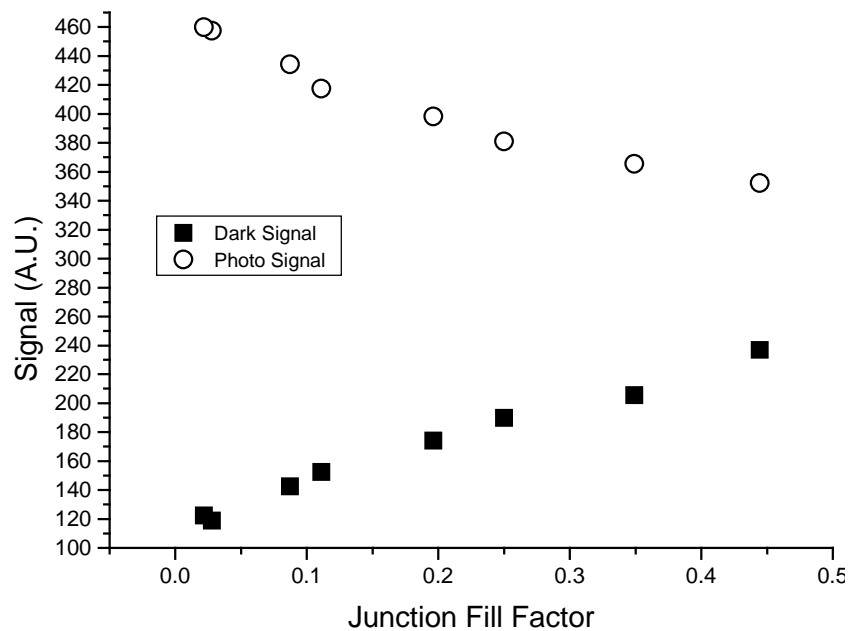


Figure 4. Dark and photo signals versus junction fill factor.

In general, a concern is that when the junction fill factor is reduced, the contrast and modulation transfer functions (CTF and MTF) will be degraded due to cross talk of signal striking the FPA between the junctions. To test this, we used the FPA described above to image a CTF test pattern (Figure 5). The test pattern had various spatial frequencies in the highest of which a stripe was imaged to match a pixel width. The image is of the raw, uncorrected video output. The dark current has not been subtracted nor has any gain nonuniformity been corrected. In the image of Figure 5, it is possible to discern the 8 horizontal sections of 16 rows each. Qualitatively, as the junction fill factor decreases from 44% (top) to 2% (bottom), there is no decrease in resolution which would be indicative of degraded CTF.

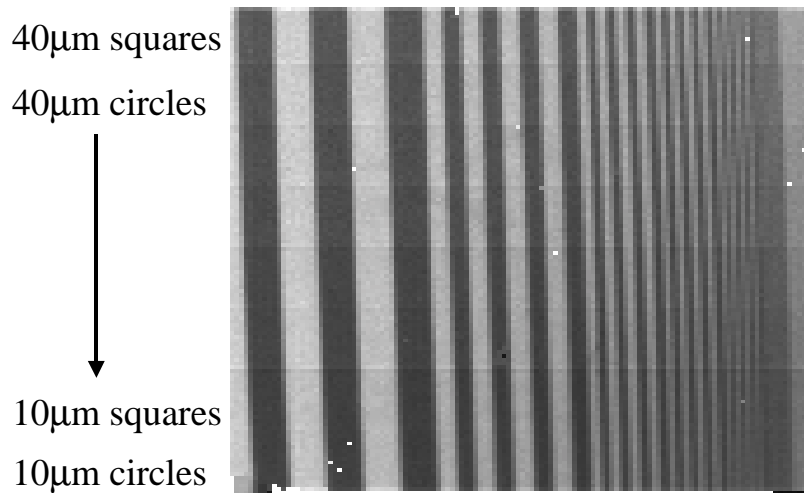


Figure 5. Contrast transfer function pattern imaged with 128x128 pixel test FPA.

The actual CTF was calculated after applying a linear two-point nonuniformity correction to the dark and bright fields associated with the image in Figure 6 and is plotted as a function of spatial frequency in Figure 6. At the higher spatial frequencies, there is substantial scatter in the data likely due to lens-related distortions. There are no quantitative differences in CTF between the various junction fill factors.

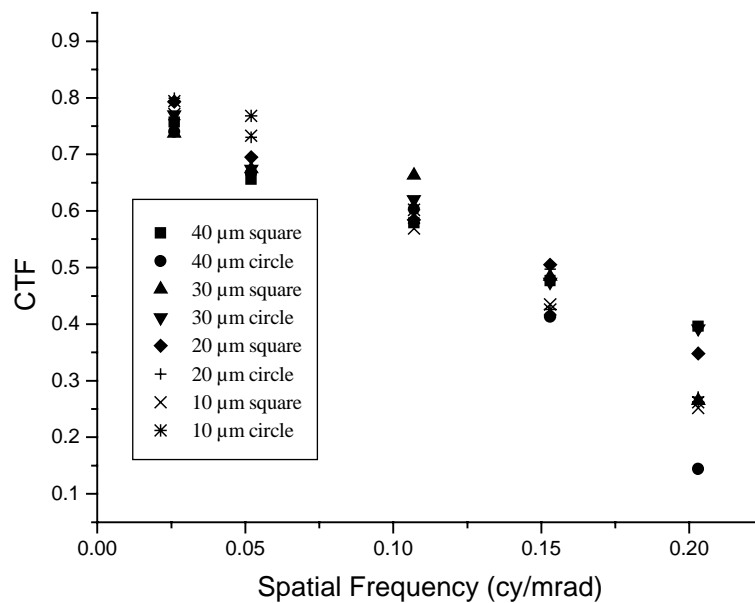


Figure 6. Contrast transfer function for the various junction geometries.

The implication of these data is that, with InGaAs FPAs, reducing the junction fill factor decreases the dark noise without reducing the photoresponse or appreciably degrading the spatial

resolution. All of the subsequent FPA results discussed in this paper were measured on devices with 12 μm diameter circular junctions. This provided increased detectivity while maintaining manufacturability.

Enhanced Detectivity using Novel Doping Profiles

The starting point for InGaAs photodiode arrays is the p-i-n structure used for telecommunication devices⁴ and illustrated in Figure 7. The $\text{In}_{0.53}\text{Ga}_{0.47}\text{As}$ absorbing layer is unintentionally doped ($1\text{-}4 \times 10^{14} \text{ cm}^{-3}$ n-type) and approximately 3 μm thick. The thickness is chosen to maximize the total absorption and the doping is low so that the entire active layer can be depleted with a 3-5 V reverse bias. This maximizes the response bandwidth both by lowering the junction capacitance and by eliminating the possibility of carrier generation beyond the depletion depth. The latter results in relatively slow drift currents. The epitaxial InP buffer layer serves to isolate the active layer from the bulk-grown InP substrate. The InP “cap” layer passivates the InGaAs surface and is typically doped $5 \times 10^{16} \text{ cm}^{-3}$ n-type. The sensitivity of high speed telecommunication diodes is often limited by signal shot noise so that dark currents below 1 nA are acceptable.

Low light level imaging ($D^* > 10^{13} \text{ cm}^{-2}\sqrt{\text{Hz/W}}$) requires dark noise-limited performance with dark currents below 1 pA. As fully-depleted operation is not required at video bandwidths (< 1 MHz), we took the approach of doping the n-type active layer to $5 \times 10^{15} \text{ cm}^{-3}$ and increasing the doping in the InP cap from $5 \times 10^{16} \text{ cm}^{-3}$ to $5 \times 10^{17} \text{ cm}^{-3}$ (Figure 7).

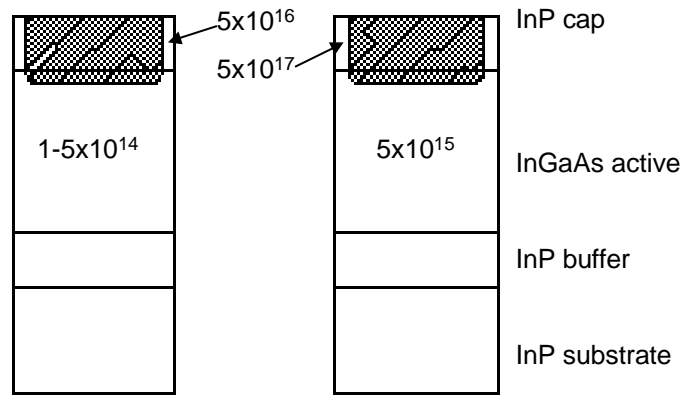


Figure 7. Standard (left) and doped (right) InGaAs p-i-n photodiode epitaxial structures.

The intentions was to lower the dark current via two mechanisms. It was hoped that the higher doping level would compensate defect states, especially those at the interfaces. Another goal was to prevent n-to-p type conversion of the InGaAs active layer along the InGaAs/InP interface during the zinc diffusion process. Zinc has been demonstrated to accumulate at the InGaAs/InP interface¹² and likely travels preferentially along the interface. This would result in a larger than expected (or needed) junction together with increased dark current.

Shunt resistance profiles of photodiode arrays fabricated with the standard and doped epitaxial structures are plotted in Figure 8. The test devices were linear arrays with $50\ \mu\text{m} \times 500\ \mu\text{m}$ pixels and the two wafers were processed together. Use of the doped structure resulted in a 5x increase in shunt resistance; from $1\text{-}2 \times 10^9\ \Omega$ to $8\text{-}9 \times 10^9\ \Omega$.

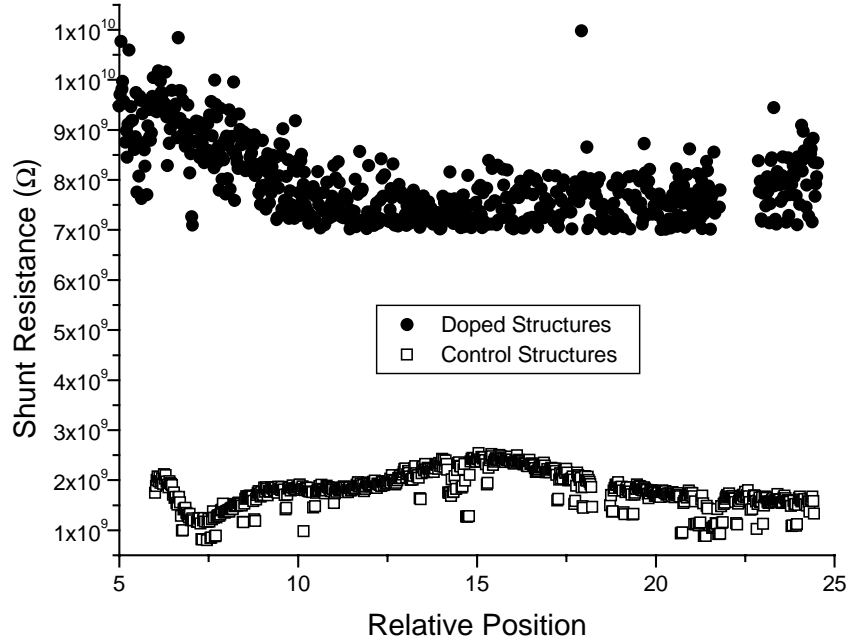


Figure 8. Shunt resistance of standard and doped linear array pixels. Each “position” contains 40 pixels.

Increased Detectivity and Low Light Level Imaging

Photodiode arrays were fabricated using the doped InGaAs structures described above. The arrays had 320×240 elements with $40\ \mu\text{m}$ pixels. The p-n junctions were $12\ \mu\text{m}$ diameter circles. The arrays were hybrid-integrated with CMOS readout integrated circuits with the gate-modulated current-mirror architecture.³ The detectivity was measured by exposing the FPA to uniform illumination using a $1.55\ \mu\text{m}$ laser diode and an integrating sphere. At $T=290\text{K}$, the mean detectivity was $3 \times 10^{14}\ \text{cm}\cdot\sqrt{\text{Hz}}/\text{W}$ and increased to $1.4 \times 10^{15}\ \text{cm}\cdot\sqrt{\text{Hz}}/\text{W}$ at 250K (Figure 9). The performance improvements resulting from the junction miniaturization and doped epitaxial layer activities are summarized in Figure 10. To the best of our knowledge, these represent the highest detectivities of any infrared material at these temperatures.

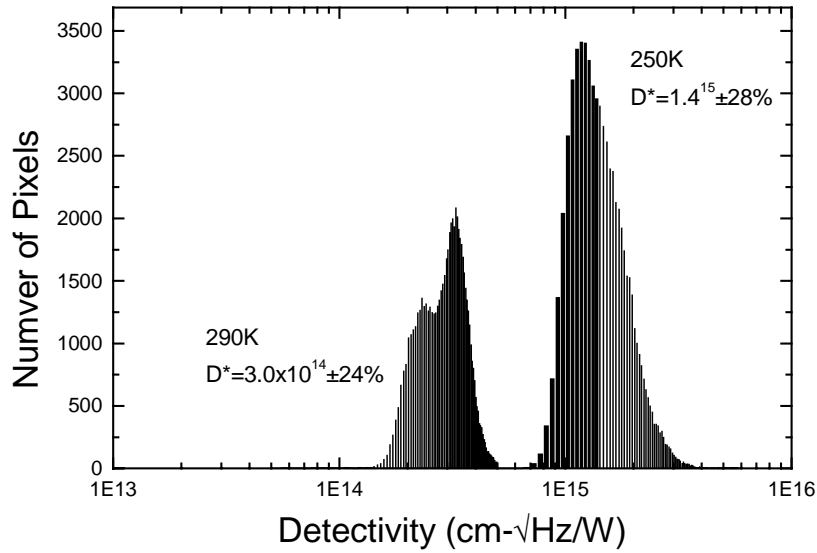


Figure 9. Detectivity histogram of 320x240 element InGaAs FPA at 250K and 290K.

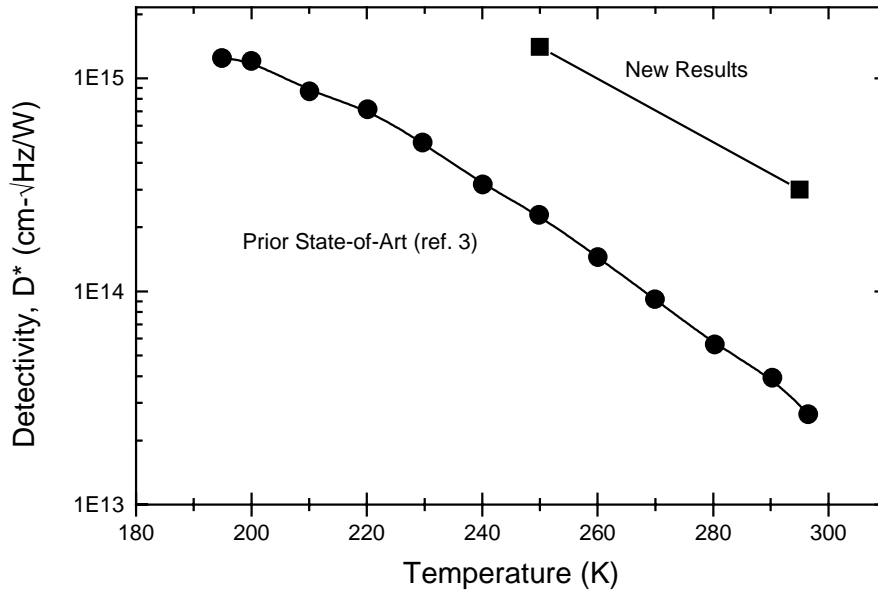


Figure 10. Summary of detectivity improvements.

Figure 11 is an image captured at night with the FPA at 250K. The conditions were overcast starlight on a moonless night. Due to background urban glow, the ambient illumination was 12 mlux, roughly equivalent to quarter moon.¹³ The image was recorded with a 75 mm visible-coated lens stopped down to f/2.8. The exposure time was 16.25 msec. A 20 mW eye-safe ($\lambda=1.55 \mu\text{m}$) laser designator was reflected off of a tree line at a distance of 500 m. The returned laser signal saturated the FPA.

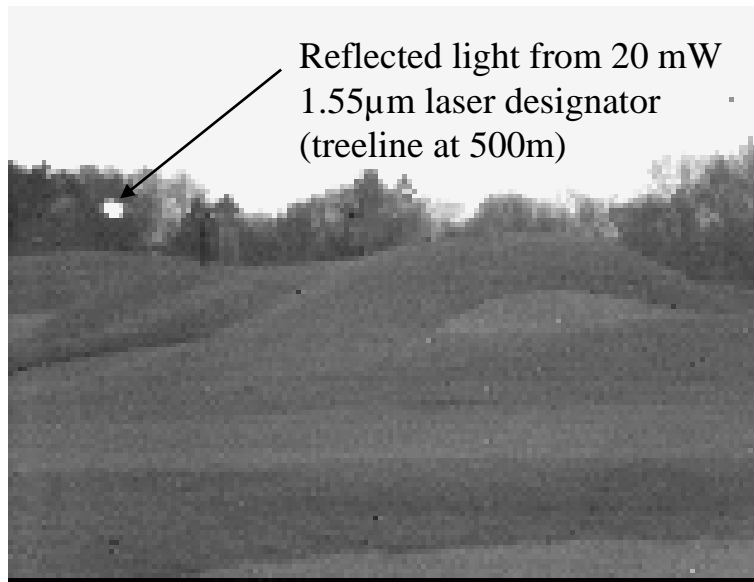


Figure 11. Image acquired with InGaAs FPA on partially overcast moonless night (FPA at 250K, 75 mm lens, f/2.8, 16.25 msec exposure, 12 mlux from urban glow).

Visible Response via Substrate Removal

InGaAs FPAs are backside-illuminated with a long wavelength cutoff due to the bandgap of the $\text{In}_{.53}\text{Ga}_{.47}\text{As}$ active layer and a $0.9\ \mu\text{m}$ “cut-on” due to absorption in the InP substrate (Figure 1). The $\text{In}_{.53}\text{Ga}_{.47}\text{As}$, itself, is sensitive to visible light. To take advantage of this visible response requires removal of the substrate.

320x240 element InGaAs photodiode arrays were fabricated using the novel heteroepitaxial structure illustrated in Figure 12. The conventional structure is shown in Figure 12a. In the modified structure (Figure 12b), two additional epitaxial layers are inserted between the InP buffer and the InGaAs active layers. A $1\ \mu\text{m}$ thick InGaAs layer was grown on the InP buffer layer. This was followed by a thin ($\leq 0.3\ \mu\text{m}$) $\text{n}^+\text{-InP}$ layer.

During the photodiode array processing, a 5:1 mixture of 25% $\text{C}_6\text{H}_8\text{O}_7$ in H_2O_2 was used to isolate the photodiode array mesa. This removed the InGaAs active layer but stopped at the thin InP “common cathode” layer.¹⁴ At this point, the photodiode arrays were hybridized to the CMOS ROICs using standard bump-bonding techniques. After hybridization, the majority of the InP substrate was removed by mechanical polishing. The remainder of InP substrate and the InP buffer layer were then removed with an $\text{HCl}:\text{H}_3\text{PO}_4$ (3:1) etch which stopped at the InGaAs “stop-etch” layer.¹⁵ The InGaAs stop-etch layer was then removed with the $\text{C}_6\text{H}_8\text{O}_7:\text{H}_2\text{O}_2$ etch stopping at the InP common cathode (Figure 12c). In the final FPA, the InGaAs photodiode array was a thin ($< 5\ \mu\text{m}$) membrane.

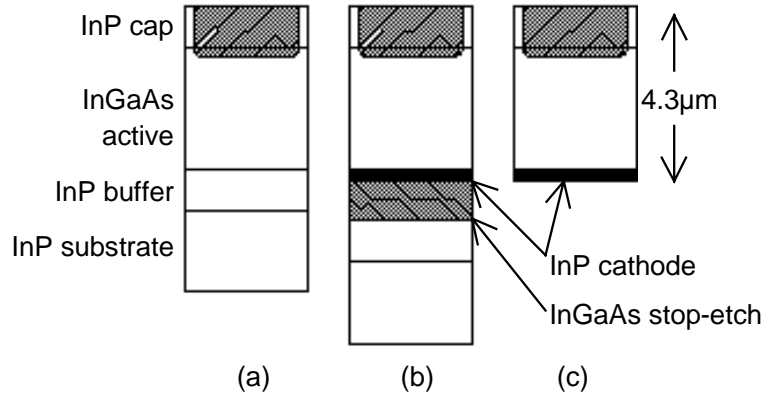


Figure 12. (a) Standard InGaAs photodiode array epitaxial structure (b) modified structure for substrate removal (c) visible response structure.

The quantum efficiencies of the InGaAs “visible response” FPA is shown in Figure 13 together with the quantum efficiencies of a backside-illuminated thick substrate FPA and a frontside-illuminated single-element p-i-n photodiode with a 1 μm thick InP cap. The differences in the curves at short wavelengths are attributable to the thicknesses of the different InP layers. In the conventional FPA, the substrate is thick (~300 μm) so the drop off below the InP cutoff (0.98 μm) is extremely sharp. The 1 μm thick cap of the frontside-illuminated photodiode allows response to a somewhat shorter wavelength (~0.8 μm) while the 0.3 μm thick common cathode of the substrate removed FPA allows response into the visible. The quantum efficiency of the substrate removed FPA was 80% at 1.5 μm, 50% at 0.8 μm and 15% at 0.5 μm.

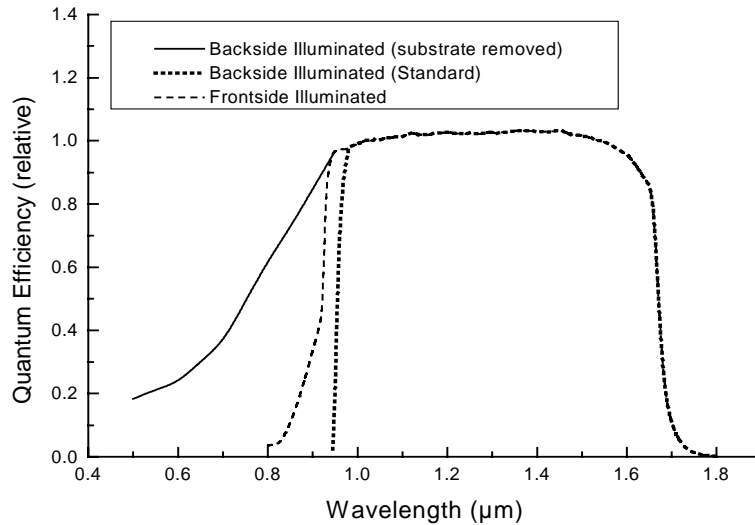


Figure 13. Quantum efficiencies of substrate-removed InGaAs FPA compared to standard FPA and frontside-illuminated photodiode.

The implications are illustrated in Figure 14 which is an image of a computer monitor captured with a substrate removed InGaAs FPA. The insets are images of the monitor captured with a visible CCD (left) and with a conventional InGaAs FPA (right). The color bars (from left to right) are red, orange, yellow, green, and blue. The monitor appears blank when viewed with the conventional FPA because the phosphors emit visible light only. As expected from the quantum efficiency measurements, all of the color bars can be seen with the substrate removed InGaAs FPA.

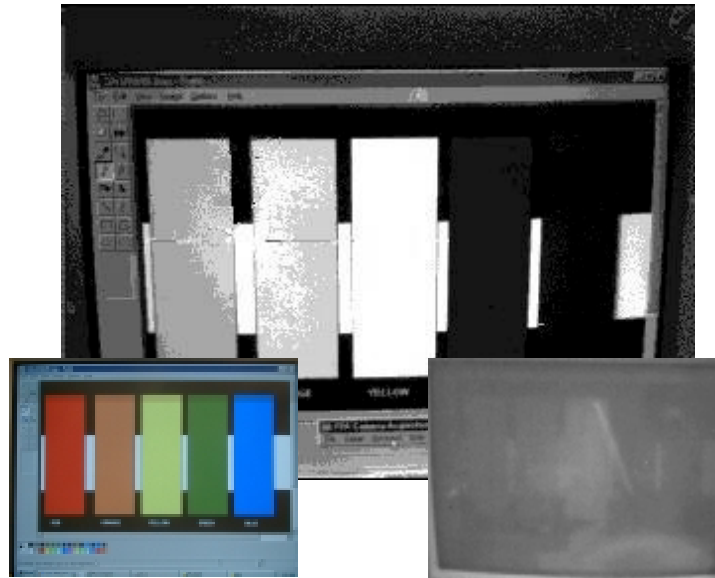


Figure 14. Computer monitor viewed with visible-response InGaAs FPA compared to silicon CCD (left) and standard InGaAs FPA (right).

2.0 SUMMARY

$\text{In}_{.53}\text{Ga}_{.47}\text{As}$ has been demonstrated to be the material of choice for imaging applications in the $0.9\ \mu\text{m}$ to $1.7\ \mu\text{m}$ band. The high detectivity at room temperature ($>10^{14}\ \text{cm}\cdot\sqrt{\text{Hz}/\text{W}}$) makes it an excellent candidate to serve as an all-solid-state alternative to $\text{I}^2\text{-CCDs}$ for night vision camera applications. Its response to eye-safe lasers opens a broad range of illumination, designation, and tracking applications. The sensitivity to both the visible and the SWIR bands both increases the broadband sensitivity and enables simultaneous visible/SWIR hyperspectral imaging.

3.0 ACKNOWLEDGEMENTS

This work has been supported by DARPA through contract DAAB07-97-C-J043, by NVESD through contract DAAB07-98-C-J010, and by NASA through contracts NAS8-98082 and NAS13-99010.

-
- ¹ “Advanced NIR Solid State Focal Plane Array”, DARPA funded Contract DAAB07-97-C-J043
- ² “Indium Gallium Arsenide Focal Plane Array and Camera for Low-Light Level 1 – 2 Micron Imaging”, DARPA funded Contract DAAB07-98-C-J010
- ³ L. J. Kozlowski, K. Vural, W. E. Kleinhans, T. Liu, G. H. Olsen, and M. J. Cohen, “Attainment of High D^* at Room Temperature via Gate-Modulated Detector Interface”, *Proc. SPIE*, **2745**, 40 (1996).
- ⁴ G. H. Olsen, and V. S. Ban, “InGaAsP: The Next Generation in Photonics Materials”, *Solid State Technology*, **30**, 99 (1987).
- ⁵ G. H. Olsen, “Long-Wavelength Components by Vapor Phase Epitaxy”, *Laser Focus World* **12**(1), 124 (1985).
- ⁶ S. R. Forrest, V. S. Ban, G. A. Gasparian, D. Gay, and G. H. Olsen, “Reliability of Vapor-Grown Planar $\text{In}_{0.53}\text{Ga}_{0.47}\text{As}/\text{InP}$ p-i-n Photodiodes with Very High Failure Activation Energy”, *IEEE Elec. Dev. Lett.* **9**, 217 (1988).
- ⁷ “100 Millimeter Semiconductor Wafer Processing Technology for InP-Based Photonic Devices” Advanced Technology Program/NIST funded Contract #70NANB8H4015
- ⁸ K. Nakajima, A. Yamaguchi, K. Akita, and T. Kotani, “Composition dependence of the band gaps of $\text{In}_{1-x}\text{Ga}_x\text{As}_{1-y}\text{P}_y$ quaternary solids lattice matched on InP substrates,” *J. Appl. Phys.* **49**, 5944 (1978).
- ⁹ M. J. Cohen, and G. H. Olsen, “Room Temperature InGaAs Camera For NIR Imaging”, *SPIE* **1946**, 436, 1993.
- ¹⁰ M. L. Vatsia, “Atmospheric Optical Environment.” *Research and Development Technical Report ECOM-7023* (1972).
- ¹¹ L. J. Kozlowski, and W. Kosonocky, “Chapter 23: Infrared Detector Arrays,” *Optics Handbook*, McGraw Hill (1995).
- ¹² P. Ambree, A. Hangleiter, M. H. Pilkuhn, and K. Wandel, “Acceptor Diffusion Across InGaAs/InP Heterointerfaces,” *Appl. Phys. Lett.* **56**, 931 (1990).
- ¹³ RCA Electro-Optics Handbook, *Technical Series EOH-10* **6**, 6 (1968).
- ¹⁴ G.C. DeSalvo, W. F. Tseng, and J. Comas, “Etch Rates and Selectivities of Citric Acid/ H_2O_2 on GaAs, $\text{Al}_3\text{Ga}_7\text{As}$, $\text{In}_2\text{Ga}_8\text{As}$, $\text{InGa}_{.53}\text{Ga}_{.47}\text{As}$, $\text{In}_{.52}\text{Ga}_{.48}\text{As}$ and InP,” *J. Electrochem. Soc.* **139** (3), 831-35 (1992).
- ¹⁵ E. Inamura, Y. Miyomoto, S. Tamura, T. Takasugi, and K. Furuya, “Wet Chemical Etching for Ultrafine Periodic Structure: Rectangular InP Corrugation of 70 nm Pitch and 100 nm Depth,” *Jpn. J. Appl. Phys.*, **28** (10), 2193-96 (1989).